Stem Cell Reports
Article

ISSCR

OPEN ACCESS

RYBP modulates embryonic neurogenesis involving the Notch signaling pathway in a PRC1-independent pattern

Qian Li,[1,2,3,8] Junchen Chen,[1,2,3,8] Feng Liang,[4,8] Jinyu Zhang,[1,2,3] Wenzheng Qu,[1,3] Xiaoli Huang,[1,3] Xuejun Cheng,[1,3] Xingsen Zhao,[1,2,3] Zhanjun Yang,[5] Shunliang Xu,[6,*] and Xuekun Li[1,2,3,7,*]

[1]The Children's Hospital, School of Medicine, Zhejiang University, Hangzhou 310052, China
[2]The Institute of Translational Medicine, School of Medicine, Zhejiang University, Hangzhou 310029, China
[3]National Clinical Research Center for Child Health, Hangzhou 310052, China
[4]The Second Affiliated Hospital, School of Medicine, Zhejiang University, Hangzhou 310002, China
[5]Department of Human Anatomy, Baotou Medical College, Baotou, 014040, China
[6]Department of Neurology, The Second Hospital, Cheeloo College of Medicine, Shandong University, Jinan 250033, China
[7]Zhejiang University Cancer Center, Zhejiang University, Hangzhou 310029, China
[8]These authors contributed equally
*Correspondence: slxu@live.com (S.X.), xuekun_li@zju.edu.cn (X.L.)
https://doi.org/10.1016/j.stemcr.2021.10.013

SUMMARY

RYBP (Ring1 and YY1 binding protein), an essential component of the Polycomb repressive complex 1 (PRC1), plays pivotal roles in development and diseases. However, the roles of Rybp in neuronal development remains completely unknown. In the present study, we have shown that the depletion of *Rybp* inhibits proliferation and promotes neuronal differentiation of embryonic neural progenitor cells (eNPCs). In addition, *Rybp* deficiency impairs the morphological development of neurons. Mechanistically, *Rybp* deficiency does not affect the global level of ubiquitination of H2A, but it inhibits Notch signaling pathway in eNPCs. The direct interaction between RYBP and CIR1 facilitates the binding of RBPJ to Notch intracellular domain (NICD) and consequently activated Notch signaling. *Rybp* loss promotes CIR1 competing with RBPJ to bind with NICD, and inhibits Notch signaling. Furthermore, ectopic Hes5, Notch signaling downstream target, rescues *Rybp*-deficiency-induced deficits. Collectively, our findings show that RYBP regulates embryonic neurogenesis and neuronal development through modulating Notch signaling in a PRC1-independent manner.

INTRODUCTION

Embryonic neurogenesis initiates with the transformation from neuroepithelial cells (NECs) to radial glial cells (RGCs), which are both identified as the fate-restricted neural progenitor cells (NPCs) (Fujita, 2003; Götz and Huttner, 2005), and is tightly regulated by multiple mechanisms, including genetic and epigenetic factors (Cao et al., 2020; Gao et al., 2020; Kriegstein and Alvarez-Buylla, 2009; Liang et al., 2020; Lim et al., 2018; Xia and Jiao, 2017; Yao et al., 2016). Histone modifiers polycomb group proteins (PcGs) form two repressive epigenetic factors, Polycomb repressive complex 1 (PRC1) and 2 (PRC2), and involves mammalian neuronal development (Desai and Pethe, 2020; Evans et al., 2020; Liu et al., 2019; Tsuboi et al., 2018, 2019). PRC1 catalyzes mono-ubiquitinated histone H2A on lysine 119 (H2AK119ub1) through Ring finger protein 1 (Ring1) A/B E3 ligases (Blackledge et al., 2015; de Napoles et al., 2004; Morey et al., 2013; Wu et al., 2013). *Ring1b* deficiency in mice also leads to embryo lethality and causes morphological defects of embryonic brain via affecting Wnt/BMP/Shh pathways (Hirabayashi et al., 2009; Morimoto-Suzki et al., 2014). *Ring1b* deficiency also inhibits self-renewal of NPCs and glial differentiation through regulating neurogenesis-related transcription factors (Eto et al., 2020; Roman-Trufero et al., 2009). In addition, the deletion of *Bmi1*, another core component of PRC1, also inhibits the proliferation of NPCs (Molofsky et al., 2003; Zencak et al., 2005). These studies together suggest the crucial role of PRC1 in neurogenesis.

Ring1 and YY1 binding protein (RYBP), a subunit of non-canonical PRC1, functions through mediating the binding of Ring1b to histone H2A and H2AK119ub1 (Tavares et al., 2012; Zhan et al., 2018). Intriguingly, RYBP can regulate gene expression through the recruitment of Oct4 to the promoter of histone lysine demethylase gene Kdm2b in a PRC1-independent pattern (Li et al., 2017a). RYBP is involved in DNA double-strand break repair, spermatogenesis, and cancer (Ali et al., 2018; Chen et al., 2009; Tian et al., 2020; Zhou et al., 2016). Furthermore, in mouse brain, RYBP interacts with Hippi to enhance caspase 8-mediated apoptosis (Stanton et al., 2007), and *Rybp* deficiency causes forebrain overgrowth and the failure of neural tube closure (Pirity et al., 2005). However, the function of RYBP and related mechanisms in regulating embryonic neurogenesis remains largely unknown.

Here, we show that RYBP is expressed in embryonic NPCs (eNPCs) and neurons during cortical development. *Rybp* deficiency inhibits the proliferation of eNPCs and promotes neuronal differentiation, but newborn neurons halt at an immature stage. Intriguingly, *Rybp* depletion did not show a significant effect on the global level of

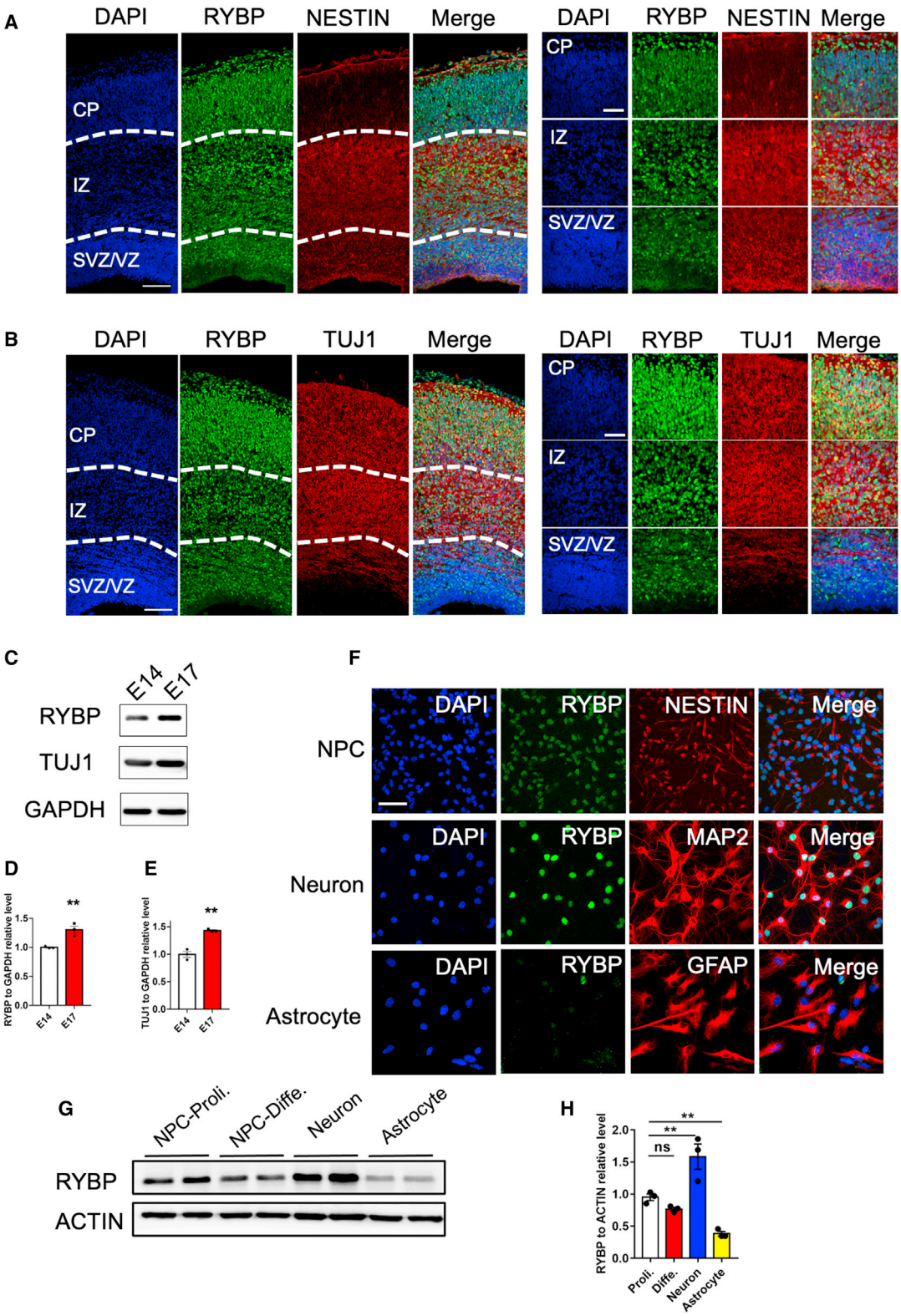

(legend on next page)

H2AK119ub1 in eNPCs. Specifically, *Rybp* knockdown (KD) increases the interaction between RBPJ-CIR1 complex and HDAC2, but decreases the binding of RBPJ to Notch intracellular domain (NICD).The reduced binding of RBPJ to NICD inhibits Notch signaling and the expression of Notch signaling downstream target *Hes5*. In addition, ectopic *Hes5* can rescue the aberrant neurogenesis induced by *Rybp* depletion. Collectively, our study reveals the essential functions of RYBP in regulating embryonic neurogenesis as an activator of the Notch signaling pathway in a PRC1-independent manner.

RESULTS

Dynamic expression of RYBP in embryonic neurogenesis

Previous studies have suggested that RYBP is expressed in eNPCs and neurons, but the expression of RYBP in eNPCs and neurons during cerebral cortex development is not clear, so we first investigated its expression pattern. Immunofluorescence staining of brain sections of embryonic mice at embryonic day 17 (E17) showed that the fluorescent signal of R RYBP was detected in both NESTIN positive (Nestin$^+$) eNPCs (Figure 1A) and β-III tubulin positive (TUJ1$^+$) neurons (Figure 1B), suggesting the extensive distribution of RYBP in embryonic mammalian brain. Western blot assay results showed that the level of RYBP increased in the cerebral cortex from E14 to E17 along with the generation of neurons (Figures 1C–1E).

Further, we isolated eNPCs and cortical neurons from the brains of E14 mice, and astrocytes from the brain of postnatal day 1 (P1) mice, respectively. The cultured eNPCs were positive for NPC markers NESTIN and SOX2 under proliferating conditions (Figure S1A), and upon differentiation induced by retinoic acid and forskolin, eNPCs generated TUJ1$^+$ neurons and GFAP$^+$ astrocytes (Figure S1B), suggesting the self-renewal and multipotent capabilities of eNPCs. The cultured cortical neurons were positive for neural cell marker MAP2 (Figure S1C). Immunostaining results showed that RYBP signal co-localized with Nestin and MAP2, respectively, and RYBP predominantly localized in the nucleus of eNPCs and neurons, whereas astrocytes had very weak RYBP signal (Figure 1F). Consistently, western blot assay results revealed that cortical neurons had the highest level of RYBP compared with proliferating and differentiated eNPCs, and astrocytes (Figures 1G and 1H).

Rybp deficiency promotes neuronal differentiation of eNPCs

To examine the roles of RYBP in regulating embryonic neurogenesis, we then performed the acute KD of *Rybp* with short hairpin RNA (shRNA) and analyzed the proliferation and differentiation capabilities of eNPCs. Western blot assay results showed the high KD efficiency of two shRNAs against *Rybp* (Figures S2A and S2B). To examine the self-renewal capability, a 5-bromo-2′-deoxyuridine (BrdU) incorporation assay was performed in the control (Ctrl) and *Rybp* KD (shRybp-1) group with proliferating eNPCs. Immunostaining and quantification results showed that *Rybp* deficiency significantly reduced the percentage of BrdU$^+$ cells (Figures 2A and 2B). *Rybp* KD also significantly reduced the number of KI-67$^+$ cells (Figures S2C and S2D). Collectively, these results suggest that *Rybp* deficiency impaired the proliferating capability of eNPCs.

To determine the effects of RYBP on the differentiation of eNPCs, eNPCs were induced for differentiation, and immunostaining with TUJ1 and GFAP antibodies was performed, respectively. We observed that *Rybp* KD significantly increased the percentage of TUJ1$^+$ neurons (Figures 2C and 2D) but reduced the percentage of GFAP$^+$ astrocytes (Figures 2E and 2F). Consistently, a dual luciferase reporter assay also showed that *Rybp* deficiency significantly increased the promoter activity of neuronal cell marker NEUROD1 (Figure 2E) and decreased the promoter activity of glial cell marker GFAP (Figure S2F). These results indicate

Figure 1. Dynamic expression of RYBP in embryonic brain

(A) Representative images of RYBP and embryonic neuronal progenitor cells (eNPCs) marker NESTIN immunostaining with brain sections of E14 embryonic mice. Scale bars, 50 μm (left; lower magnification) and 100 μm (right; higher magnification). SVZ, subventricular zone; VZ, ventricular zone; IZ, intermediate zone; CP, cortical plate.

(B) Representative images of RYBP and neuronal cell marker TUJ1 immunostaining with brain sections of embryonic mice. Scale bars, 50 μm (left; lower magnification) and 100 μm (right; higher magnification).

(C–E) Western blot (C) and quantification results showing the protein levels of RYBP (D) and TUJ1 (E) in the cerebral cortex of E14 and E17 mouse brains, respectively. n = 3 independent experiments for each group. Data are presented as mean ± SEM. Unpaired t test; *p < 0.05; **p < 0.01.

(F) Representative images of RYBP immunostaining in NESTIN$^+$ eNPCs, MAP2$^+$ neurons, and GFAP$^+$ astrocytes, respectively. Scale bar, 50 μm.

(G and H) Western blot (G) and quantification results (H) showing that the levels of RYBP in eNPCs, neurons, and astrocytes. Actin was used as an internal control. n = 3 independent experiments for each group. Data are presented as mean ± SEM. Unpaired t test; *p < 0.05; **p < 0.01.

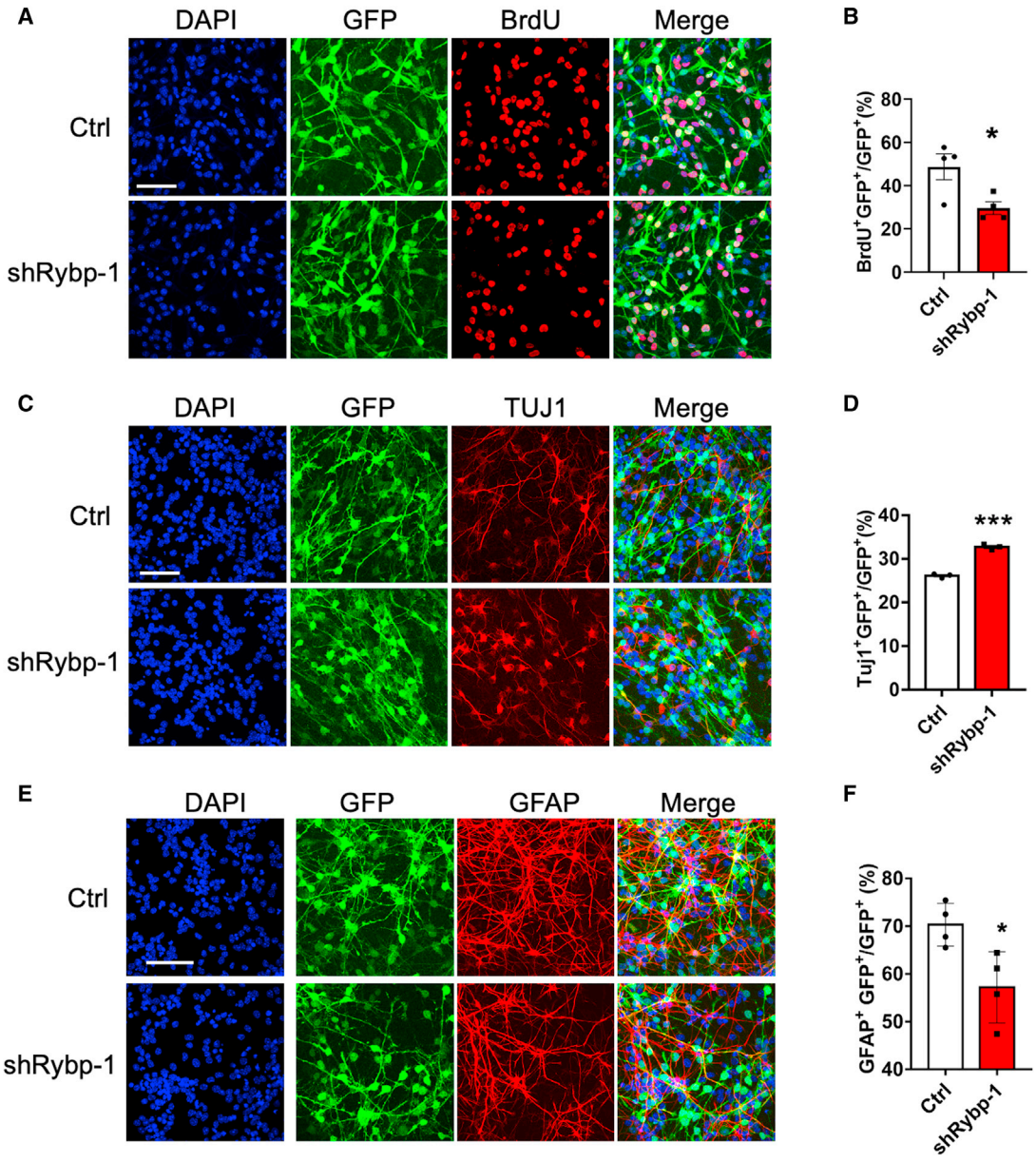

Figure 2. *Rybp* deficiency inhibits the proliferation, but promotes neuronal differentiation, of eNPCs *in vitro*

(A) Representative images of BrdU immunostaining with eNPCs infected with lentivirus expressing GFP-scramble (control [Ctrl]) and GFP-sh*Rybp* (sh*Rybp*), respectively. Scale bar, 50 μm.

(B) The quantification results of GFP^+BrdU^+ cells in control and *Rybp* KD eNPCs. *Rybp* KD reduced the proliferative ability of eNPCs. n = 4 independent experiments for each group. Data are presented as mean ± SEM, unpaired t test; *p < 0.05; **p < 0.01; ***p < 0.001.

(C) Representative images of neuronal cell marker TUJ1 immunostaining with control and *Rybp* KD eNPCs under proliferating conditions. Scale bar, 50 μm.

(D) Quantification of $TUJ1^+GFP^+$ cells in control and *Rybp* KD eNPCs under proliferating conditions. n = 3 independent experiments for each group. Data are presented as mean ± SEM, unpaired t test; *p < 0.05; **p < 0.01; ***p < 0.001.

(E) Representative images of neuronal cell marker TUJ1 immunostaining with control and *Rybp* KD eNPCs at differentiation condition. Scale bar, 50 μm.

(F) Quantification of $TUJ1^+GFP^+$ cells in control and *Rybp* KD eNPCs at differentiation condition. n = 3 independent experiments for each group. Data are presented as mean ± SEM, unpaired t test; *p < 0.05; **p < 0.01; ***p < 0.001.

(legend continued on next page)

that the lack of *Rybp* skews eNPCs to differentiate toward a neuronal lineage with an inhibition of glial lineage.

To examine the function of RYBP in regulating embryonic neurogenesis *in vivo*, we performed *in utero* electroporation (IUE) to deliver scramble and sh*Rybp* plasmids into the brain of E14 embryonic mice, respectively, which were sacrificed and analyzed on E17. Immunostaining of BrdU and GFP showed that the percentage of $BrdU^+GFP^+$/GFP^+ cells decreased in ventricular zone/subventricular zone (VZ/SVZ) in *Rybp* KD group (shRybp) (Figures 3A and 3B), suggesting the inhibited proliferation of eNPCs. The percentage of $PAX6^+$ RGCs, one type of NPC, also decreased in VZ/SVZ in *Rybp* KD group (Figures 3C and 3D). In addition, the percentage of $TBR2^+$ intermediate progenitor cells (IPCs), one type of neuronal progenitor cell, increased in VZ/SVZ (Figures 3E and 3F), but the percentage of $TUJ1^+$ neurons significantly increased at the cortical plate (CP) region in the *Rybp* KD group (Figures 3G and 3H). Collectively, these results suggest that *Rybp* deficiency inhibits the self-renewal capability of eNPCs and promotes neuronal differentiation *in vitro* and *in vivo*.

Rybp deficiency inhibits the morphological development of neurons

Next, we examined the roles of RYBP in regulating the morphological development of neurons. We performed IUE experiment and observed that *Rybp* KD significantly decreased the number of GFP^+ cells in the CP region (Figures S3A–S3D). Morphological analysis of GFP^+ cells in CP showed that *Rybp* KD significantly reduced the length of dendrites and the number of intersections (Figures 4A–4C). In addition, *Rybp* KD also reduced the total length of dendrites and the number of dendritic intersections of newborn neurons generated from the differentiation of eNPCs (Figures 4D–4F). Sholl analysis revealed the decreased dendritic complexity in *Rybp* KD group compared with the Ctrl group (Figure 4G). We further performed *Rybp* KD in cultured cortical neurons at DIV 4 and DIV 14, respectively. Three days after plasmid transfection, neurons were harvested for analysis. We observed that *Rybp* deficiency consistently resulted in a decreased complexity of dendrites in primary neurons at both time points (Figures 4H–4O). Meanwhile, we did not observe a significant effect of *Rybp* KD on the cell survival according to TUNEL staining assay (Figures S3E and S3F). Collectively, these results indicate that *Rybp* depletion inhibits the morphological development of neurons.

RYBP regulates Notch signaling in eNPCs

To elucidate the molecular mechanisms by which RYBP regulates embryonic neurogenesis, we performed an RNA sequencing (RNA-seq) assay with Ctrl and *Rybp* KD eNPC samples, which were infected with lentivirus expressing scramble (Ctrl) and shRNA against *Rybp* (shRybp), respectively. Pearson correlation analysis on intra-group samples showed a relatively high correlation ($R > 0.9$, $p < 2.2 \times 10^{-16}$) between the two biological duplicates of each group (Figure S4A).

Given that RYBP is an essential component of the Polycomb repressive complex 1 (PRC1), and mediates histone H2A ubiquitination on lysine 119 (H2AK119ub1), we speculated that *Rybp* KD should display overall promoting effects on gene expression. However, RNA-seq data analysis showed that more genes were downregulated in the *Rybp* KD group than were upregulated (922 downregulated genes versus 544 upregulated genes) (Figure 5A; Table S1). Gene Ontology (GO) enrichment analysis of the differentially expressed genes (DEGs) suggested that the downregulated genes, but not the upregulated genes, highly enriched in terms related to neurogenesis and neural development (Figure 5B). Kyoto Encyclopedia of Genes and Genomes (KEGG) analysis showed that the downregulated genes were involved in the pathways related to neural development, such as axon guidance, glutamatergic synapse, calcium signaling pathway, and synaptic vesicle cycle (Figure 5C). Furthermore, we did not observe a significant change in the global level of H2AK119ub1 in *Rybp* KD eNPCs (Figures 5D and 5E), which was consistent in embryonic stem cells (ESCs) (Rose et al., 2016; Zhao et al., 2020), suggesting additional mechanisms by which RYBP functions other than mediating H2AK119ub1.

Furthermore, we analyzed chromatin immunoprecipitation sequencing (ChIP-seq) data from *Rybp* knockout and control mouse ESCs generated recently (SRR11014805, SRR11014806, SRR11014835, and SRR11014836)[29], and found that the motif for RBPJ appeared in RYBP ChIP-seq data (Figure S4B), suggesting a direct or indirect interaction between RYBP and RBPJ. To determine the relationship between RYBP, CIR1, and RBPJ, ectopic Cir1 and Rbpj plasmids were transfected into Neuro2a cells followed by co-immunoprecipitation and western blot assays, respectively. We observed that CIR1 (hemagglutinin [HA]-CIR1), but not RBPJ (FLAG-RBPJ), could easily precipitate RYBP (Figures 5F and 5G), suggesting that RYBP directly interacts with CIR1, but not RBPJ.

(G) Representative images of astrocyte cell marker GFAP immunostaining with control and *Rybp* KD eNPCs at differentiation condition. Scale bar, 50 μm.

(H) Quantification of $GFAP^+GFP^+$ cells in control and *Rybp* KD eNPCs at differentiation condition. n = 3 independent experiments for each group. Data are presented as mean ± SEM, unpaired t test; *p < 0.05; **p < 0.01; ***p < 0.001.

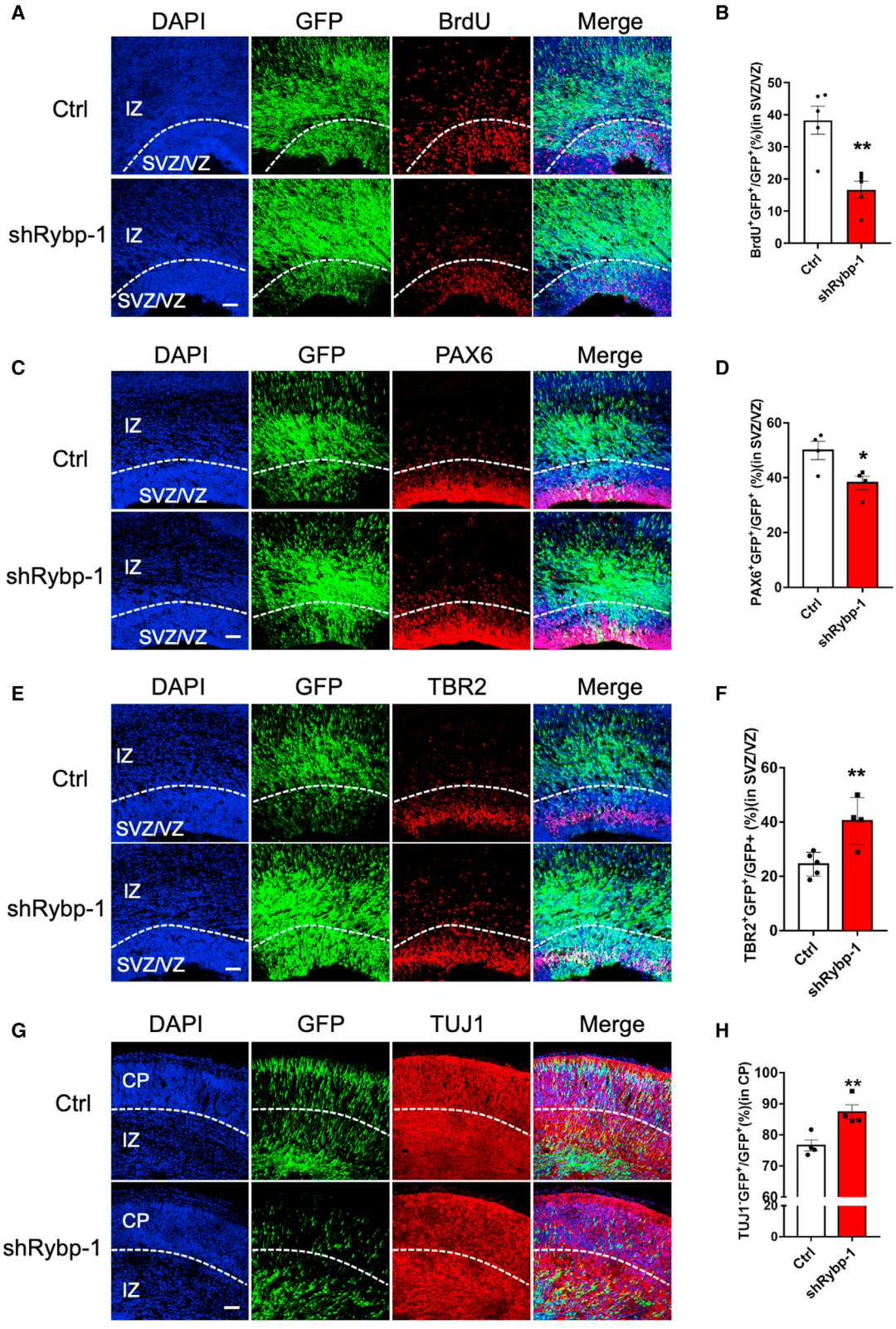

(legend on next page)

Previous studies have shown that RBPJ and CIR1 could form a complex that recruits HDAC and consequently regulates gene expression, including Notch signaling pathway (Hsieh et al., 1999; Pajerowski et al., 2009). We next analyzed the fragments per kilobase of transcript per million (FPKM) values of Notch signaling components based on the RNA-seq data, and observed that *Rybp* KD did not significantly alter the expression of *Notch1–3* and *Rbpj* at the transcriptional level (Figure S4C). However, the expression of some Notch ligands, such as *Dll1* and *Dll3*, decreased, but *Jag1* increased in the *Rybp* KD group (Figure S4D). Interestingly, *Hes5*, one of the downstream targets of Notch signaling, decreased in the *Rybp* KD group compared with the Ctrl group (Figure S4E). The altered expression of these transcripts was also determined with quantitative real-time PCR (qRT-PCR) (Figures S4F–S4R). Western blot assay results showed that *Rybp* KD did not affect the level of NOTCH1 but significantly decreased the level of HES5 (Figures 5H–5J). Together, these results suggest that *Rybp* deficiency disturbs Notch signaling and consequently inhibits the expression of its downstream targets.23

Rybp KD represses Notch signaling as a competitive inhibitor of CIR1/RBPJ complex formation

Given that *Rybp* deficiency did not affect the expression level of the Notch receptor, but physically associated with CIR1, we hypothesized that RYBP inhibited Notch signaling via regulation of the CIR1/RBPJ complex. To test this hypothesis, we co-transfected ectopic CIR1 (HA-CIR1) and RBPJ (FLAG-RBPJ) with scramble and sh*Rybp* plasmids in N2a cells, respectively. Co-immunoprecipitation followed by western blot assay showed that Rybp deficiency enhanced the physical interaction between CIR1 and RBPJ in N2a cells (Figures 6A and 6B). Since CIR1/RBPJ complex could recruit HDAC, we then examined the association between HDAC2 and RBPJ and observed that *Rybp* KD significantly increased the interaction between HDAC2 and RBPJ in N2a cells (Figures 6C and 6D).

Next, we examined the effects of *Rybp* KD on the interaction between NICD and RBPJ. Co-immunoprecipitation followed by western blot assay showed that that *Rybp* KD significantly decreased the interaction between NICD and RBPJ in N2a cells (Figures 6E and 6F). In addition, we observed that *Rybp* deficiency decreased the levels of histone H3 on lysine 27 acetylation (H3K27Ac) and total H3 acetylation, but not histone H3 on lysine 27 methylation (H3K27me3) in eNPCs (Figures 6G–6J). In addition, ectopic NICD and RBPJ could restore the expression of several key components of Notch signaling pathway under *Rybp* KD condition in eNPCs cells, respectively (Figures S5A–S5G). Collectively, these results suggest that RYBP could bind with CIR1 in competition with RBPJ. Under *Rybp* depletion condition, more RBPJ could bind with CIR1 and recruit HDAC2, which consequently inhibited gene expression.

Ectopic *Hes5* rescues the neurogenesis deficits induced by *Rybp* KD

Next, we aimed to examine whether promoting Notch signaling could rescue the abnormal neurogenesis induced by *Rybp* depletion. We performed the electroporation of ectopic Hes5 in eNPCs. BrdU immunostaining and quantification results showed that ectopic Hes5 could significantly increase the percentage of $BrdU^+$ cells in *Rybp* KD eNPCs (Figures 7A and 7B). In addition, ectopic HES5 could reduce the excessive neurons induced by *Rybp* KD upon the differentiation of eNPCs (Figures 7C and 7D). Morphological analysis showed that ectopic HES5 could significantly increase the total length of dendrites, the number of intersections, and the dendritic complexity (Figures 7E–7H). qRT-PCR results showed that ectopic *Hes5* could significantly restore the expression of Notch signaling pathway

Figure 3. *Rybp* deficiency represses the proliferation, but promotes neuronal differentiation of eNPCs *in vivo*

(A) Representative images of BrdU immunostaining with control and *Rybp* KD brain sections. Scramble and sh*Rybp* plasmids were delivered into the brain via *in utero* electroporation at E14, and mice were sacrificed for assay at E17. BrdU was injected (100 mg/kg, intraperitoneally [i.p.]) 2 h prior to the sacrifice. Scale bar, 50 μm.

(B) The quantification results showed the percentage of GFP^+BrdU^+/GFP^+ in SVZ/VZ layer decreased in *Rybp* KD group. n = 5 independent experiments for each group. Data are presented as mean ± SEM, unpaired t test; *p < 0.05; **p < 0.01; ***p < 0.001.

(C) Representative images of radial glial marker PAX6 immunostaining with control and *Rybp* KD brain sections. Scramble and sh*Rybp* plasmids were delivered into the brain with *in utero* electroporation at E14 and mice were sacrificed for assay at E17. Scale bar, 50 μm.

(D) The quantification results showed the percentage of GFP^+PAX6^+/GFP^+ in SVZ/VZ layer decreased in *Rybp* KD group. n = 4 independent experiments for each group. Data are presented as mean ± SEM, unpaired t test; *p < 0.05; **p < 0.01; ***p < 0.001.

(E) Representative images of intermediate progenitor marker TBR2 immunostaining with control and *Rybp* KD brain sections. Scale bar, 50 μm.

(F) The quantification results showed the percentage of GFP^+TBR2^+/GFP^+ in SVZ/VZ layer increased in *Rybp* KD group. n = 5 independent experiments for each group. Data are presented as mean ± SEM, unpaired t test; *p < 0.05; **p < 0.01; ***p < 0.001.

(G) Representative images of neuronal cell marker TBR2 immunostaining with control and *Rybp* KD brain sections. Scale bar, 50 μm.

(H) The quantification results showed that the percentage of GFP^+TUJ1^+/GFP^+ in CP layer increased in *Rybp* KD group. n = 5 independent experiments for each group. Data are presented as mean ± SEM, unpaired t test; *p < 0.05; **p < 0.01; ***p < 0.001.

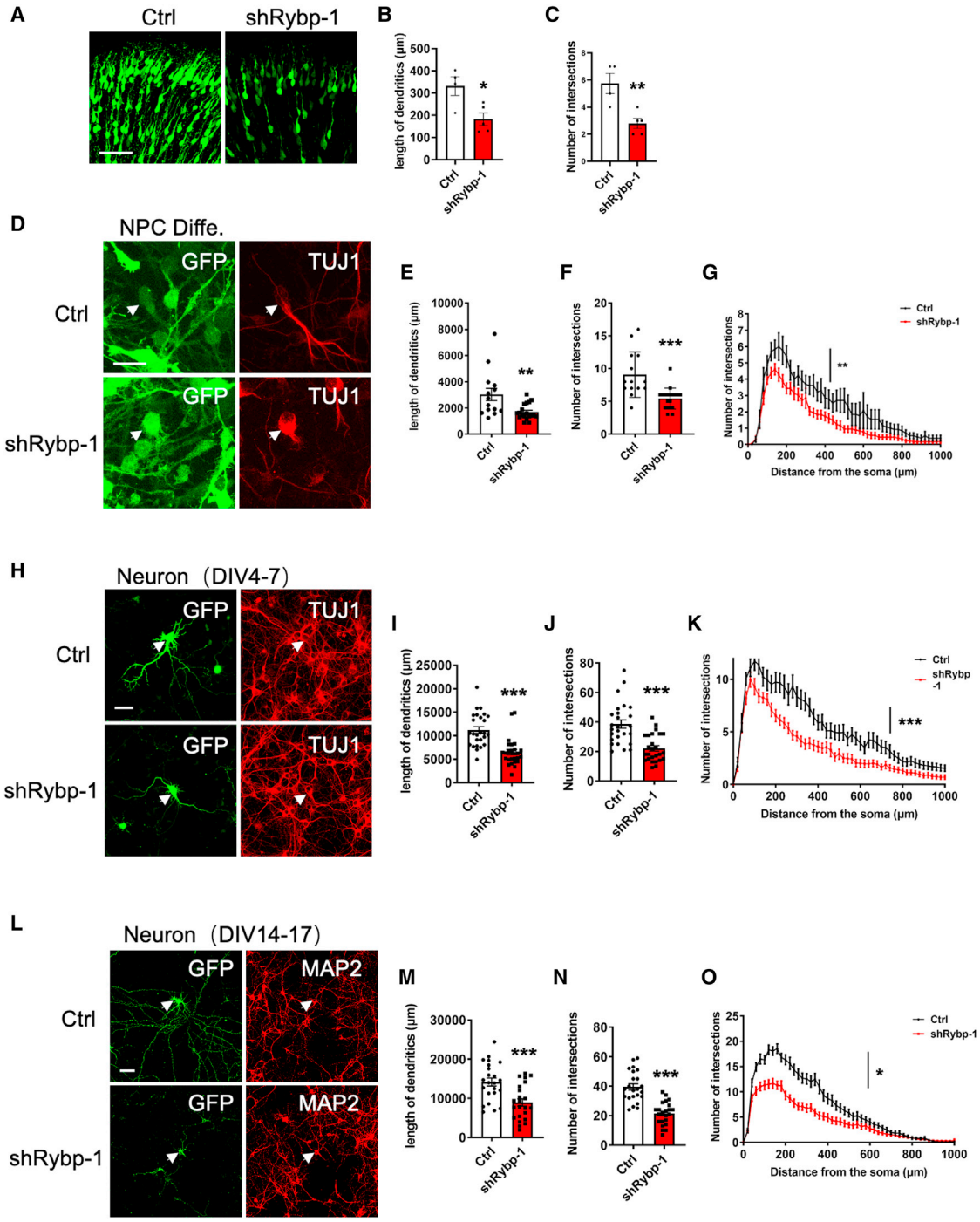

Figure 4. *Rybp* deficiency inhibits morphological development of neurons

(A) Representative images of GFP$^+$ cells in control and *Rybp* KD brain sections. Scramble and sh*Rybp* plasmids were delivered into the brain via *in utero* electroporation at E14 and mice were sacrificed for assay at E17. Scale bar, 50 μm.

(B and C) The quantification results showed that the length of dendrites (B) and the number of branch points (C) both significantly decreased in the *Rybp* KD group compared with control group. n = 4 independent experiments for control group and n = 5 for *Rybp* KD group. Data are presented as mean ± SEM, unpaired t test; *p < 0.05; **p < 0.01; ***p < 0.001.

(D) Representative images of newborn neurons (TUJ1$^+$) generated from the differentiation of eNPCs. Scale bar, 50 μm.

(legend continued on next page)

components, including *Notch1*, *Dll1*, *Dll3*, *Jag1*, and *Jag2*, in eNPCs under *Rybp* KD condition (Figures S5H–S5N). Collectively, these results suggest that enhancing Notch signaling by ectopic Hes5 can rescue the abnormal neurogenesis and neuronal development induced by *Rybp* depletion.

DISCUSSION

Mammalian embryonic neurogenesis is orchestrated by diverse genetic and epigenetic mechanisms, which coordinate the responses to extracellular cues and control the multiple stages of neurogenesis, including the proliferation and differentiation of eNPCs and fate determination of newborn neurons (Yao et al., 2016). In the present study, we have showed that *Rybp* depletion represses the proliferation and promotes neural differentiation of eNPCs, inhibits the morphological development of newborn neurons, and consequently leads to aberrant neurogenesis in mice. Mechanistically, RYBP modulates the Notch signaling pathway as the competitive inhibitor of RBPJ in a PRC1-independent manner. The *Rybp*-depletion-induced aberrant neurogenesis could be rescued by restoring Notch signaling.

Consistent with recent studies that have showed that RYBP inhibits the passive dilution of H2AK119ub1 during cell division and exerts an influence on its abundance (Rose et al., 2016; Zhao et al., 2020), our present results showed that *Rybp* depletion did not affect the global level of H2AK119ub1 in eNPCs. We speculate that the neurogenesis deficits caused by *Rybp* KD are not due to the overall decrease of H2AK119ub1 in eNPCs. In line with this speculation, RNA-seq data analysis has showed that *Rybp* deficiency did not display overall promoting effects on gene expression in eNPCs, but inhibits gene expression. Consistent with this, *Rybp* KD significantly decreases the level of histone H3 acetylation, a marker for active gene expression. In ESCs, ChIP-seq data have shown that around 30% of RYBP enrichment sites did not overlap with H2AK119ub1 sites (Zhao et al., 2020). These results suggest that RYBP directly or indirectly acts a transcription regulator.

Notch signaling plays important roles in maintaining the stemness of neural stem/progenitor cells and regulating neurogenesis (Basak and Taylor, 2007; Chen et al., 2021; de la Pompa et al., 1997; Gaiano and Fishell, 2002; Hatakeyama et al., 2004; Stump et al., 2002). Once Notch signaling is activated, NICD is released and competitively binds to RBPJ. The NICD/RBPJ complex promotes the expression of its target genes, such as *Hes5* and *Hey1*, via mediating histone acetylation (Castel et al., 2013; Kopan and Ilagan, 2009; Oswald et al., 2001). The inhibition of the Notch signaling pathway reduces cell proliferation and increases neuronal differentiation in the embryonic cerebral cortex, resulting in focal cortical dysplasia (Cotter et al., 1999; Lasky and Wu, 2005; Zhang et al., 2018). In ESCs, *Rybp* deficiency reduces the level of H2AK119ub1 and promotes the expression of Notch1 (Zhao et al., 2020). In eNPCs, *Ring1b* depletion inhibits Notch signaling without affecting H2AK119ub1 and transcriptional level of Notch receptors (Roman-Trufero et al., 2009). Our present data suggested a direct interaction between RYBP and CIR1, but not RYBP and RBPJ. We speculated that the

(E and F) The quantification results showed that the length of dendrites (E) and the number of branch points (F) were both significantly decreased in *Rybp* KD neurons compared with control group. n = 14 cells from three brains for control group and n = 19 cells from three brains for *Rybp* KD group. Data are presented as mean ± SEM, unpaired t test; *p < 0.05; **p < 0.01; ***p < 0.001.

(G) Sholl analysis results showed that *Rybp* KD reduced the dendritic complexity of cortical neurons compared with control group. n = 14 cells from three brains for control group and n = 19 cells from three brains for *Rybp* KD group. Data are presented as mean ± SEM, unpaired t test; *p < 0.05; **p < 0.01; ***p < 0.001.

(H) Representative images of cultured cortical neurons at DIV 7. Primary neurons were isolated from the cerebral cortex of E15 mice brain and transfected with control and sh*Rybp* plasmids at DIV 4, respectively. Cells were collected for assay at DIV 7. Scale bar, 50 μm.

(I and J) The quantification results showed that *Rybp* KD significantly decreased the length of dendrites (I) and the number of branch points (J) of cortical neurons compared with control group. n = 14 cells from three brains for control group and n = 19 cells from three brains for *Rybp* KD group. Data are presented as mean ± SEM, unpaired t test; *p < 0.05; **p < 0.01; ***p < 0.001.

(K) Sholl analysis results showed that *Rybp* KD reduced the dendritic complexity of cortical neurons compared with control group. n = 14 cells from three brains for control group and n = 19 cells from three brains for *Rybp* KD group. Data are presented as mean ± SEM, unpaired t test; *p < 0.05; **p < 0.01; ***p < 0.001.

(L) Representative images of cultured cortical neurons at DIV 17. Cultured neurons were transfected with control or sh*Rybp* plasmid at DIV 14 and collected for assay at DIV 17, respectively. Scale bar, 50 μm.

(M and N) The quantification results showed that the length of dendrites (M) and the number of branch points (N) were both significantly decreased in *Rybp* KD group compared with control group. n = 23 cells from three brains for each group. Data are presented as mean ± SEM, unpaired t test; *p < 0.05; **p < 0.01; ***p < 0.001.

(O) Sholl analysis results showed that *Rybp* KD reduced the dendritic complexity of neurons compared with control group. n = 23 cells from three brains for each group. Data are presented as mean ± SEM, unpaired t test; *p < 0.05; **p < 0.01; ***p < 0.001.

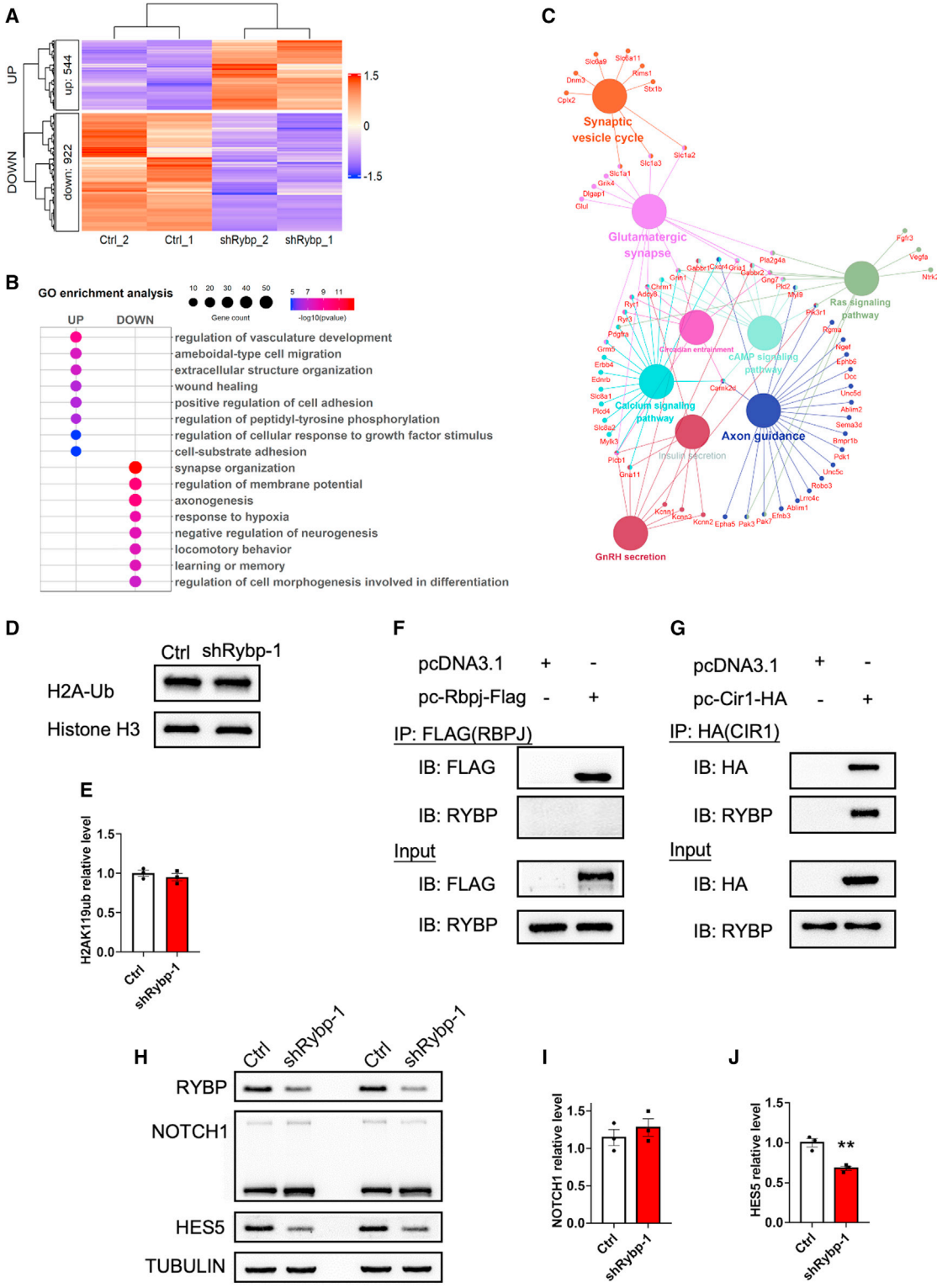

Figure 5. *Rybp* KD alters transcriptome and inhibits Notch signaling in eNPCs

(A) The heatmap showing DEG between control and *Rybp* KD eNPCs.

(B) GO analysis showed that the downregulated genes in *Rybp* KD eNPCs were highly enriched for the terms related with neuronal development.

(legend continued on next page)

observed RBPJ motif in RYBP ChIP-seq data in mESCs could be due to the interaction between RYBP and CIR1, and CIR1 and RBPJ. The interaction between RYBP and CIR1 facilitated the binding of RBPJ to NICD and consequently activated Notch signaling; the loss of *Rybp* promoted CIR1 competing with RBPJ to bind with NICD, and consequently inhibited Notch signaling. Therefore, our findings suggest that RYBP serves as a critical regulator of Notch signaling during neurogenesis.

In summary, our present study has revealed the important function of RYBP in regulating embryonic neurogenesis. The interaction between RYBP and CIR1 affects the binding of RBPJ to NICD in a PRC1-independent pattern, and consequently regulates Notch signaling pathway.

EXPERIMENTAL PROCEDURES

Mice

C57BL/6 pregnant mice were purchased from Shanghai Laboratory Animal Center (SLAC). Mice were housed on a 12-h light/dark schedule and fed *ad libitum*. All experiments were conducted following the protocols approved by The Animal Ethics Committee of Zhejiang University.

Isolation and culture of embryonic NPCs

The isolation of eNPCs was performed as described previously (Li et al., 2017b; Szulwach et al., 2010). Briefly, the cerebral cortex of mice (E14) was dissected and cut into small pieces. Tissue samples were treated with 0.1% Trypsin at 37°C for 5 min, and the enzyme digestion was stopped with FBS. After washing with DMEM/F-12 basal medium, cells were cultured with DMEM/F-12 medium containing 2% B27 (minus vitamin A), 20 ng/mL EGF, 20 ng/mL FGF-2, 2 mM L-glutamine, and 1% antibiotic-antimycotic in a 5% CO_2 incubator at 37°C. The medium was half replaced every 2 days. eNPCs usually grew up around 2 weeks under proliferating conditions, and were passaged about three or four times. The homogeneity of eNPCs was determined by immunostaining with lineage-specific markers.

To perform the proliferation and differentiation assay, eNPCs were plated onto the coated coverslips with proliferation medium. For the proliferation assay, eNPCs were cultured with fresh proliferation medium containing 5 μM BrdU for 4 h. For the differentiation assay, eNPCs were cultured with DMEM/F-12 medium containing 2% B27 (minus vitamin A), 2 mM L-glutamine, 1% antibiotic-antimycotic, 1 μM retinoic acid, and 5 μM forskolin (differentiation medium) for 48 h. At the scheduled time point, eNPCs were fixed with 4% paraformaldehyde (PFA) followed by immunostaining with proper antibodies. The information for the used primary and secondary antibodies can be found in Table S2.

BrdU labeling and immunostaining

BrdU (100 mg/kg) was administered to pregnant mice 1.5 h before the sacrifice. Pregnant mice were anesthetized with isoflurane and transcardially perfused with cold phosphate-buffered saline (PBS) followed by cold 4% PFA. The brains of embryonic mice were dissected and post-fixed with 4% PFA overnight. After being completely dehydrated with 30% sucrose at 4°C, brain samples were embedded with optimal cutting temperature (OCT) compound and coronally sectioned at a thickness of 20 μm with a cryostat (Leica). The sections were stored in preservative solution at −20°C.

To perform immunostaining, mouse brain sections were washed with PBS for 30 min. Cultured cells were washed with 1× PBS, fixed in 4% PFA in 1× PBS for 30 min, and then were incubated with blocking buffer (3% goat serum and 0.1% Triton X-100 in 1× PBS) for 1 h at room temperature. Sections were incubated with primary antibodies at 4°C overnight. For BrdU immunostaining, the sections were pretreated with 1M HCl and incubated at 37°C for 30 min. After being washed three times with PBS, tissue and cell samples were incubated with DAPI (4′,6-diamidino-2-phenylindole) and fluorescence-labeled secondary antibodies for 1 h. Samples were viewed and images were taken with Olympus confocal microscope (Olympus IX83-FV3000).

Plasmid transfection

shRNAs targeting mouse Rybp (#1, 5′-GATCCTCCTAGTGAAGC TAAC-3′; #2, 5′-CAGCAGTGAATGATGAATCTT-3′) and scramble shRNA (5′-TTCTCCGAACGTGTCACGT-3′) were cloned into the pLKO.1 vector and pSicoR vector (Li and Jiao, 2020), respectively. For the overexpression of Rybp, Cir1, Rbpj, NICD, and Hes5, the mouse cDNA was amplified and cloned to pcDNA3.1(+) vector. Half volume of medium was changed with fresh medium 6 h before the transfection. Five hours later, the maintaining medium was replaced with neurobasal medium, and 3 μg of lentivirus vector plasmids was mixed with 4 μL of lipo2000 in 200 μL of neurobasal medium. Thirty minutes later, the mixture was added to one well of a 24-well plate. The medium was replaced with fresh maintaining medium 4 h after transfection.

Co-immunoprecipitation assay

For co-immunoprecipitation, cells were lysed with co-immunoprecipitation lysis buffer (50 mM Tris-HCl [pH 7.8], 150 mM KCl, 0.1%

(C) KEGG analysis showed that downregulated genes were involved in pathways relating to neuronal development.
(D and E) Western blot (D) and quantification (E) showed that *Rybp* KD did not alter the level of H2AK119ub1 in eNPCs compared with control group. n = 3 independent experiments for each group. Data are presented as mean ± SEM, unpaired t test; *p < 0.05; **p < 0.01; ***p < 0.001.
(F) Immunoprecipitation followed by western blot assay showed that RYBP did not directly interact with RBPJ (FLAG-RBPJ) in N2a cells.
(G) Immunoprecipitation followed by western blot assay showed that RYBP physically interacted with CIR1 (HA-CIR1) in N2a cells.
(H–J) Western blot (H) and quantification results showed that *Rybp* KD did not significantly alter the level of Notch1 (I), but significantly decreased the level of HES5 (J) in eNPCs. TUBULIN was used as an internal control. n = 3 independent experiments for each group. Data are presented as mean ± SEM, unpaired t test; *p < 0.05; **p < 0.01; ***p < 0.001.

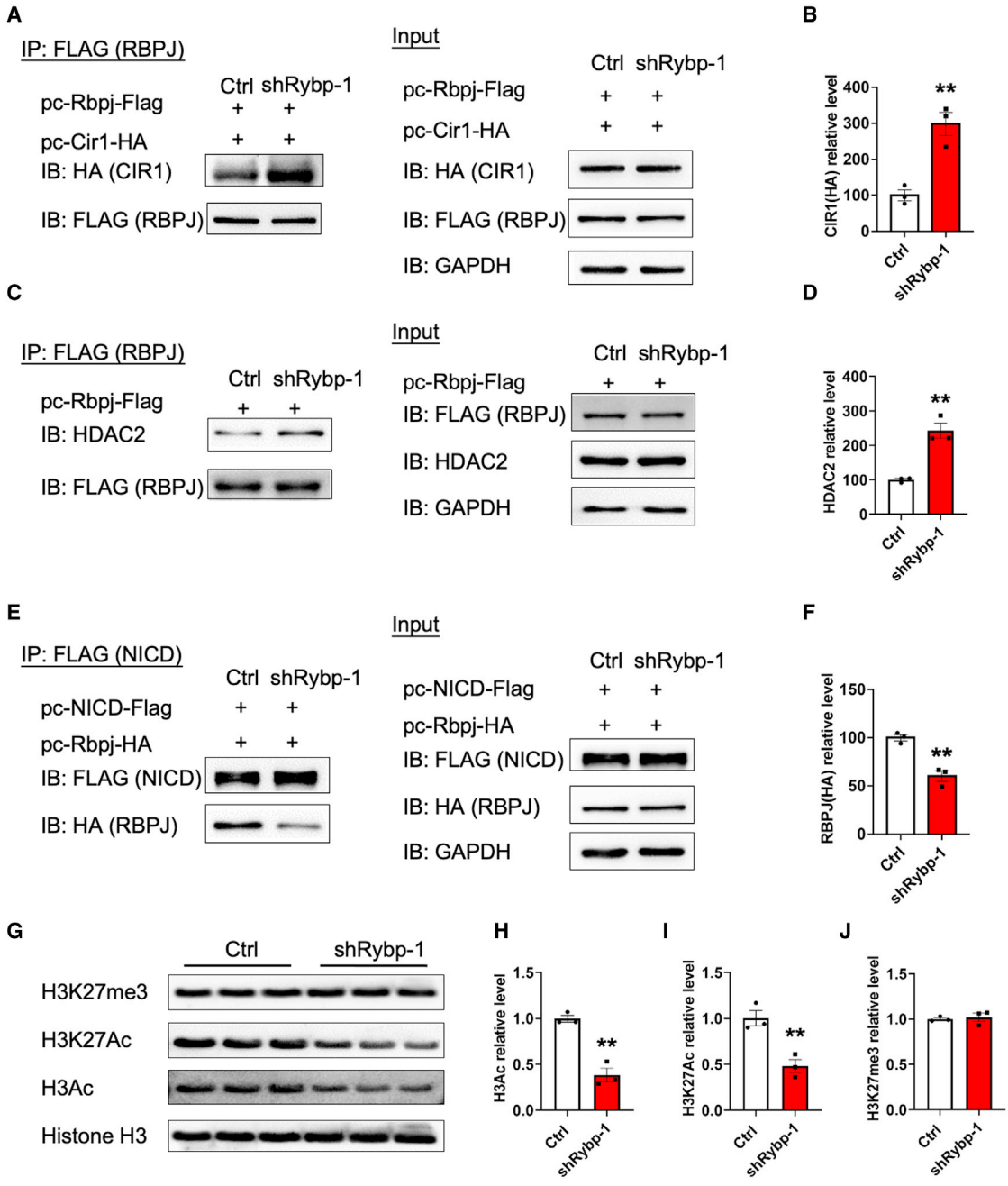

Figure 6. RYBP promotes Notch signaling as a competitive inhibitor of CIR1/RBPJ complex formation

(A and B) Immunoprecipitation followed by western blot assay (A) and quantification results (B) showed that *Rybp* KD significantly increased the physical interaction between RBPJ (FLAG-RBPJ) and CIR1 (HA-CIR1) in N2a cells. n = 3 independent experiments for each group. Data are presented as mean ± SEM, unpaired t test; *p < 0.05; **p < 0.01; ***p < 0.001.

(C and D) Immunoprecipitation followed by western blot assay (C) and quantification results (D) showed that *Rybp* KD increased the physical interaction between RBPJ (FLAG-RBPJ) and Hdac2 in N2a cells. n = 3 independent experiments for each group. Data are presented as mean ± SEM, unpaired t test; *p < 0.05; **p < 0.01; ***p < 0.001.

(legend continued on next page)

Triton X, 5mM EDTA) containing one protease inhibitor cocktail on ice for 30 min. The supernatant was directly incubated with anti-FLAG M2 magnetic beads or anti-HA magnetic beads overnight at 4°C. The second day, samples were washed with washing buffer (50 mM Tris-HCl [pH 7.8], 150 mM KCl, 0.01% Triton X, 5 mM EDTA) containing 1× protease inhibitor cocktail three times. Then, the beads were resuspended with 30 μL of RIPA buffer and 10 μL of 4× loading buffer, and denatured for 5 min at 100°C, followed by immunoblotting assays.

Electroporation and luciferase assays

Electroporation was performed as described previously (Szulwach et al., 2010). Briefly, around 2 × 10^6 eNPCs were resuspended in 100 μL of nucleofection solution and electroporated according to the manufacturer's protocol. For each electroporation, 4 μg of scramble or shRybp plasmids, 0.1 μg of Renilla-luciferase plasmids, and 2 μg of NeuroD1- or Gfap-luciferase plasmids were used, respectively. The cells were further cultured with fresh proliferation medium, and the medium was replaced with differentiation medium on the second day. Forty-eight hours later, cells were collected for a dual luciferase assay with a luminometer according to the manufacturer's protocol.

In utero electroporation

The detailed protocols of *in utero* electroporation have been described previously (Li and Jiao, 2020; Saito, 2006). The C57BL/6 pregnant mice (E14) were anesthetized by inhaled isoflurane (RWD). Two microliters of recombinant plasmid (final concentration 1 μg/μL) mixed with Venus-GFP at a ratio of 3:1 and fast green (0.01%) were manually microinjected into the fetal lateral ventricle using a glass capillary (Hirschmann DE-M 16). For electroporation, the uterine horns were exposed and five 100-μspulses of 35 V at 900-μsintervals were delivered across the uterus using an electroporator (BEX, SN. 101438). After electroporation, the pregnant mice were killed at E17. Fetuses were perfused with PBS, followed by perfusion of 4% PFA. Fetal brains were gently removed and post-fixed in 4% PFA overnight at 4°C. Twenty-four hours later, the brain samples were transferred into 30% sucrose solution at 4°C for 24 h. The brain tissue was embedded in OCT (Thermo Fisher Scientific) and sectioned in the coronal plane (15 μm) with a cryostat. Brain sections were analyzed by confocal microscopy (OLYMPUS IX83-FV3000 2019, Olympus, Japan), and the numbers of GFP-positive or multi-marker co-labeled cells in distinct brain regions were quantified using ImageJ software.

Isolation and culture of primary neurons and astrocytes

The fetal cortex was dissected from the brain of E15 mice pups and treated with 0.25% trypsin at 37°C for 30 min. Around 150,000 cortical neurons were plated onto a cell climbing slice (Corning) coated with poly-D-lysine (5 μg/mL, Sigma, P0899-10). Neurons were cultured with DMEM (Gibco, 11095-080) supplemented with 10% FBS (Gibco, 10091-148), 1% L-Glu (Gibco, 5030-149), and 1% sodium pyruvate (Gibco, 11360-070) for 4 h. The medium was replaced with neurobasal medium (Gibco, 21103-049) supplemented with 2% B27 (Gibco, 17504-044), 0.25% L-Glu (Gibco, 25030-149), and 0.125% Glutamax (Thermo, 35050061).

Neonatal mice (postnatal day 1–3) were sacrificed, and cortical and hippocampi regions were dissected out under a microscope. The tissues were digested with 0.25% trypsin (Gibco, 25200072) for 25 min at 37°C to dissociate into single cell suspensions. About 1 × 10^7 cells were plated onto one poly-D-lysine-coated T25 culture flask with DMEM medium supplemented with 10% FBS, 1% antibiotic-antimycotic, and 2 mM L-glutamine, and the medium was replaced every 2 days. After culture for 7–10 days, samples were put on a shaker (240 rpm) for 12 h at 37°C, and the medium was completely replaced with fresh culture medium.

Culture of Neuro2a cells

Neuroblastoma (Neuro2a) cells were cultured with DMEM medium containing 10% FBS, 2 mM L-glutamine, and 1% antibiotic-antimycotic in a 5% CO_2 incubator at 37°C, and medium was replaced every 24 h.

Total RNA extraction and qRT-PCR

Total RNA was extracted from the control and *Rybp* KD eNPCs, respectively, by TRIzol reagent according to the manufacture's protocol, and the concentration was determined with a NanoDrop spectrophotometer 2000 (Thermo Fisher Scientific); 0.5 μg of total RNA was used for reverse transcription, and qRT-PCR assays were performed using SYBR Green (Vazyme) in triplicate. The results were analyzed using the $^{\Delta\Delta}$Ct method. The used primers for qRT-PCR are shown in Table S3.

RNA-seq and data analysis

All samples used for the cDNA library were assessed by NanoDrop 2000 (Thermo Fisher Scientific), and the RNA integrity value (RIN) was determined with the RNA Nano 6000 Assay Kit of the Bioanalyzer 2100 system (Agilent Technologies). A total amount of 3 μg of RNA per sample was used as input. Sequencing libraries were generated following the manufacturer's recommendations, and index codes were added to attribute sequences to each sample using NEBNext Ultra™ RNA Library Prep Kit for Illumina (NEB).

Raw reads of fastq format were processed. Clean reads were mapped to mm10 using Hisat2 v2.0.5, and only uniquely mapped reads were used for further analysis. FeatureCounts v2.0.1 was used to count the read numbers mapped to each gene, and FPKM of each transcript was calculated based on the length of the gene and

(E and F) Immunoprecipitation followed by western blot assay (E) and quantification results (F) showed that *Rybp* KD significantly decreased the physical interaction between NICD (FLAG-NICD) and RBPJ (HA-RBPJ) in N2a cells. n = 3 independent experiments for each group. Data are presented as mean ± SEM, unpaired t test; *p < 0.05; **p < 0.01; ***p < 0.001.

(G–J) Western blot assay (G) and quantification results (H–J) showed that *Rybp* KD significantly decreased the levels of H3Ac (H) and H3K27Ac (I), but not altered the level of H3K27me3 (J) in eNPCs. n = 3 for each group. Data are presented as mean ± SEM, unpaired t test; *p < 0.05; **p < 0.01; ***p < 0.001.

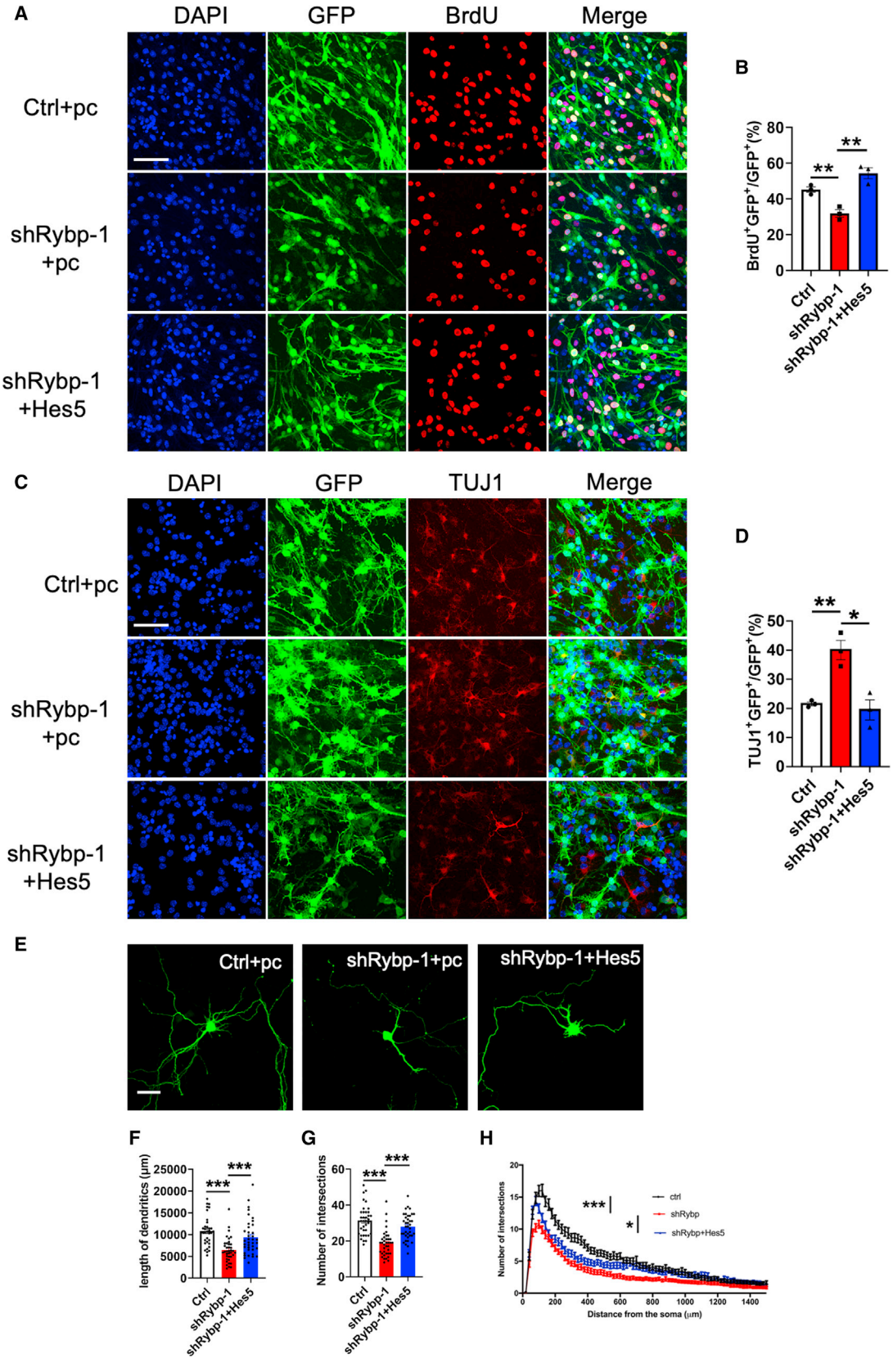

(legend on next page)

read counts mapped to this gene. Pearson correlations were performed on all samples. The differential expression genes between samples were analyzed with edge2. A p value of 0.05 and absolute fold change of 1.5 were set as the threshold for significantly differential expression.

Western blot

Cortex tissues or cells were dissected on ice and quick-frozen in liquid nitrogen before total protein extraction. Tissues were triturated with cold radio immunoprecipation assay (RIPA) lysis buffer on ice and transferred to a microfuge tube, followed by centrifugation at 4°C for 30 min at 12,000 rpm. Cell pellets were collected and the total proteins were lysed with cold RIPA lysis buffer on ice and then centrifuged at 4°C for 30 min at 12,000 rpm. Supernatants were collected and quantified by bicinchoninic acid (BCA) protein assay. Samples were subjected to sodium dodecyl sulfate-polyacrylamide gel electrophoresis (SDS-PAGE) at different concentrations of separating gels according to molecular weights of target proteins, and then transferred onto nitrocellulose membranes. Membranes were blocked with 5% non-fat milk or 5% BSA in Tris-HCl buffer with 0.1% Tween (pH 7.6) at room temperature for 1 h and incubated with primary antibodies at 4°C overnight. After washing with TBST three times, membranes were incubated with horseradish peroxidase (HRP)-labeled secondary antibodies at room temperature for 1 h. Membranes were washed three times with TBST and incubated with UltraSignal ECL. The signal was detected by Tanon 5200 Detection system, and the intensity of images was analyzed with Adobe Photoshop software.

Statistical analysis

All data are presented as mean ± SEM and were analyzed with GraphPad Prism software (GraphPad Software, CA). For statistical analyses of cell distribution and labeling *in vivo*, three to five embryos were analyzed for each condition and at least three sections were examined for each embryo. For comparisons between two groups, a two-tailed unpaired Student's t test was used. A value of $p < 0.05$ was considered statistically significant (statistical significance: n.s., not significant; *$p < 0.05$; **$p < 0.01$; ***$p < 0.001$).

Data and code availability

The accession number for the RNA-seq data reported in this paper is GEO: GSE174147.

SUPPLEMENTAL INFORMATION

Supplemental information can be found online at https://doi.org/10.1016/j.stemcr.2021.10.013.

AUTHOR CONTRIBUTIONS

X.L. conceptualized the project. Q.L. and J.C. did cell isolation and culture, immunofluorescence staining, qRT-PCR, immunoprecipitation, and western blot with the help of F.L., J.Z., and X.Z. Q.L. did *in utero* electroporation with the help of X.H. W.Q. performed RNA-seq data analysis. Q.L. performed the quantification of immunofluorescence staining with the help of X.C. and X.Z. X.L. wrote the manuscript with the help of Q.L., Z.Y., and S.X. All authors reviewed and approved the final manuscript.

CONFLICTS OF INTEREST

The authors declare no competing interests.

ACKNOWLEDGMENTS

This work was supported in part by the National Key Research and Development Program of China (2017YFE0196600 to X.L.) and the National Natural Science Foundation of China (grants 81901676 to F.L., 92049108 to X.L.). S.X. is supported by Shandong Provincial Natural Science Foundation, China

Figure 7. Ectopic *Hes5* rescues the neuronal deficits induced by *Rybp* KD

(A) Representative images of BrdU immunostaining with eNPCs transfected with scramble + vector (Ctrl + pc), sh*Rybp* + vector (sh*Rybp* + pc), and sh*Rybp* + *Hes5* plasmids, respectively. Scale bar, 50 μm.

(B) Quantification results showed that ectopic *Hes5* could rescue the decreased self-renewal capability of eNPCs induced by *Rybp* KD, which was indicated by the percentage of $BrdU^+$ cells. n = 3 independent experiments for each group. Data are presented as mean ± SEM, unpaired t test; *$p < 0.05$; **$p < 0.01$; ***$p < 0.001$.

(C) Representative images of TUJ1 immunostaining with the differentiated eNPCs. After transfection with scramble + vector (Ctrl + pc), sh*Rybp* + vector (sh*Rybp* + pc), and shRybp + Hes5 plasmids, respectively, eNPCs were induced for differentiation for 2 days. Scale bar, 50 μm.

(D) Quantification results showed that ectopic *Hes5* could inhibit the excessive neuronal differentiation induced by *Rybp* KD, which was indicated by the percentage of $TUJ1^+$ cells. n = 3 independent experiments for each group. Data are presented as mean ± SEM, unpaired t test; *$p < 0.05$; **$p < 0.01$; ***$p < 0.001$.

(E) Representative images of cortical neurons transfected with scramble + vector (Ctrl + pc), sh*Rybp* + vector (sh*Rybp* + pc), and sh*Rybp* + *Hes5* plasmids at DIV 4, respectively, and collected for assay at DIV 7. Scale bar, 50 μm.

(F and G) The quantification results showed that ectopic *Hes5* significantly increased the length of dendrites (F) and the number of branch points (G) of cortical neurons, which were significantly decreased by *Rybp* KD. n = 34 cells from three brains for control group, n = 33 cells from three brains for *Rybp* KD group, and n = 38 cells from three brains for *Rybp* KD + *Hes5* group. Data are presented as mean ± SEM, unpaired t test; *$p < 0.05$; **$p < 0.01$; ***$p < 0.001$.

(H) Sholl analysis results showed that ectopic Hes5 significantly increased the dendritic complexity of cortical neurons. n = 34 cells from three brains for control group, n = 33 cells from three brains for *Rybp* KD group, and n = 38 cells from three brains for *Rybp* KD + *Hes5* group. Data are presented as mean ± SEM, unpaired t test; *$p < 0.05$; **$p < 0.01$; ***$p < 0.001$.

(ZR2015HM024, 2019GSF108066), Independent Innovation Foundation of Shandong University (IIFSDU), and Scientific Research Foundation for the Returned Overseas Chinese Scholars, State Education Ministry, China (SRF for ROCS, SEM).

Received: June 11, 2021
Revised: October 20, 2021
Accepted: October 21, 2021
Published: November 18, 2021

REFERENCES

Ali, M.A.M., Strickfaden, H., Lee, B.L., Spyracopoulos, L., and Hendzel, M.J. (2018). RYBP is a K63-ubiquitin-chain-binding protein that inhibits homologous recombination repair. Cell Rep. *22*, 383–395.

Basak, O., and Taylor, V. (2007). Identification of self-replicating multipotent progenitors in the embryonic nervous system by high Notch activity and Hes5 expression. Eur. J. Neurosci. *25*, 1006–1022.

Blackledge, N.P., Rose, N.R., and Klose, R.J. (2015). Targeting polycomb systems to regulate gene expression: modifications to a complex story. Nat. Rev. Mol. Cell Biol. *16*, 643–649.

Cao, Y., Zhuang, Y., Chen, J., Xu, W., Shou, Y., Huang, X., Shu, Q., and Li, X. (2020). Dynamic effects of Fto in regulating the proliferation and differentiation of adult neural stem cells of mice. Hum. Mol. Genet. *29*, 727–735.

Castel, D., Mourikis, P., Bartels, S.J., Brinkman, A.B., Tajbakhsh, S., and Stunnenberg, H.G. (2013). Dynamic binding of RBPJ is determined by Notch signaling status. Genes Dev. *27*, 1059–1071.

Chen, D., Zhang, J., Li, M., Rayburn, E.R., Wang, H., and Zhang, R. (2009). RYBP stabilizes p53 by modulating MDM2. EMBO Rep. *10*, 166–172.

Chen, J., Dong, X., Cheng, X., Zhu, Q., Zhang, J., Li, Q., Huang, X., Wang, M., Li, L., Guo, W., et al. (2021). Ogt controls neural stem/progenitor cell pool and adult neurogenesis through modulating Notch signaling. Cell Rep. *34*, 108905.

Cotter, D., Honavar, M., Lovestone, S., Raymond, L., Kerwin, R., Anderton, B., and Everall, I. (1999). Disturbance of Notch-1 and Wnt signalling proteins in neuroglial balloon cells and abnormal large neurons in focal cortical dysplasia in human cortex. Acta Neuropathol. *98*, 465–472.

de la Pompa, J.L., Wakeham, A., Correia, K.M., Samper, E., Brown, S., Aguilera, R.J., Nakano, T., Honjo, T., Mak, T.W., Rossant, J., et al. (1997). Conservation of the Notch signalling pathway in mammalian neurogenesis. Development *124*, 1139–1148.

de Napoles, M., Mermoud, J.E., Wakao, R., Tang, Y.A., Endoh, M., Appanah, R., Nesterova, T.B., Silva, J., Otte, A.P., Vidal, M., et al. (2004). Polycomb group proteins Ring1A/B link ubiquitylation of histone H2A to heritable gene silencing and X inactivation. Dev. Cell *7*, 663–676.

Desai, D., and Pethe, P. (2020). Polycomb repressive complex 1: regulators of neurogenesis from embryonic to adult stage. J. Cell Physiol. *235*, 4031–4045.

Eto, H., Kishi, Y., Yakushiji-Kaminatsui, N., Sugishita, H., Utsunomiya, S., Koseki, H., and Gotoh, Y. (2020). The Polycomb group protein Ring1 regulates dorsoventral patterning of the mouse telencephalon. Nat. Commun. *11*, 5709.

Evans, M.K., Matsui, Y., Xu, B., Willis, C., Loome, J., Milburn, L., Fan, Y., Pagala, V., and Peng, J.C. (2020). Ybx1 fine-tunes PRC2 activities to control embryonic brain development. Nat. Commun. *11*, 4060.

Fujita, S. (2003). The discovery of the matrix cell, the identification of the multipotent neural stem cell and the development of the central nervous system. Cell Struct. Funct. *28*, 205–228.

Gaiano, N., and Fishell, G. (2002). The role of notch in promoting glial and neural stem cell fates. Annu. Rev. Neurosci. *25*, 471–490.

Gao, H., Cheng, X., Chen, J., Ji, C., Guo, H., Qu, W., Dong, X., Chen, Y., Ma, L., Shu, Q., et al. (2020). Fto-modulated lipid niche regulates adult neurogenesis through modulating adenosine metabolism. Hum. Mol. Genet. *29*, 2775–2787.

Götz, M., and Huttner, W.B. (2005). The cell biology of neurogenesis. Nat. Rev. Mol. Cell Biol. *6*, 777–788.

Hatakeyama, J., Bessho, Y., Katoh, K., Ookawara, S., Fujioka, M., Guillemot, F., and Kageyama, R. (2004). Hes genes regulate size, shape and histogenesis of the nervous system by control of the timing of neural stem cell differentiation. Development *131*, 5539–5550.

Hirabayashi, Y., Suzki, N., Tsuboi, M., Endo, T.A., Toyoda, T., Shinga, J., Koseki, H., Vidal, M., and Gotoh, Y. (2009). Polycomb limits the neurogenic competence of neural precursor cells to promote astrogenic fate transition. Neuron *63*, 600–613.

Hsieh, J.J., Zhou, S., Chen, L., Young, D.B., and Hayward, S.D. (1999). CIR, a corepressor linking the DNA binding factor CBF1 to the histone deacetylase complex. Proc. Natl. Acad. Sci. U. S. A. *96*, 23–28.

Kopan, R., and Ilagan, M.X. (2009). The canonical Notch signaling pathway: unfolding the activation mechanism. Cell *137*, 216–233.

Kriegstein, A., and Alvarez-Buylla, A. (2009). The glial nature of embryonic and adult neural stem cells. Annu. Rev. Neurosci. *32*, 149–184.

Lasky, J.L., and Wu, H. (2005). Notch signaling, brain development, and human disease. Pediatr. Res. *57*, 104R–109R.

Li, H., Lai, P., Jia, J., Song, Y., Xia, Q., Huang, K., He, N., Ping, W., Chen, J., Yang, Z., et al. (2017a). RNA helicase DDX5 inhibits reprogramming to pluripotency by miRNA-based repression of RYBP and its PRC1-dependent and -independent functions. Cell Stem Cell *20*, 462–477 e466.

Li, X., Yao, B., Chen, L., Kang, Y., Li, Y., Cheng, Y., Li, L., Lin, L., Wang, Z., Wang, M., et al. (2017b). Ten-eleven translocation 2 interacts with forkhead box O3 and regulates adult neurogenesis. Nat. Commun. *8*, 15903.

Li, Y., and Jiao, J. (2020). Deficiency of TRPM2 leads to embryonic neurogenesis defects in hyperthermia. Sci. Adv. *6*, eaay6350.

Liang, Q., Su, L., Zhang, D., and Jiao, J. (2020). CD93 negatively regulates astrogenesis in response to MMRN2 through the transcriptional repressor ZFP503 in the developing brain. Proc. Natl. Acad. Sci. U. S. A. *117*, 9413–9422.

Lim, L., Mi, D., Llorca, A., and Marín, O. (2018). Development and functional diversification of cortical interneurons. Neuron *100*, 294–313.

Liu, P.P., Xu, Y.J., Dai, S.K., Du, H.Z., Wang, Y.Y., Li, X.G., Teng, Z.Q., and Liu, C.M. (2019). Polycomb protein EED regulates neuronal differentiation through targeting SOX11 in hippocampal dentate gyrus. Stem Cel. Rep. *13*, 115–131.

Molofsky, A.V., Pardal, R., Iwashita, T., Park, I.K., Clarke, M.F., and Morrison, S.J. (2003). Bmi-1 dependence distinguishes neural stem cell self-renewal from progenitor proliferation. Nature *425*, 962–967.

Morey, L., Aloia, L., Cozzuto, L., Benitah, S.A., and Di Croce, L. (2013). RYBP and Cbx7 define specific biological functions of polycomb complexes in mouse embryonic stem cells. Cell Rep. *3*, 60–69.

Morimoto-Suzki, N., Hirabayashi, Y., Tyssowski, K., Shinga, J., Vidal, M., Koseki, H., and Gotoh, Y. (2014). The polycomb component Ring1B regulates the timed termination of subcerebral projection neuron production during mouse neocortical development. Development *141*, 4343–4353.

Oswald, F., Täuber, B., Dobner, T., Bourteele, S., Kostezka, U., Adler, G., Liptay, S., and Schmid, R.M. (2001). p300 acts as a transcriptional coactivator for mammalian Notch-1. Mol. Cell. Biol. *21*, 7761–7774.

Pajerowski, A.G., Nguyen, C., Aghajanian, H., Shapiro, M.J., and Shapiro, V.S. (2009). NKAP is a transcriptional repressor of notch signaling and is required for T cell development. Immunity *30*, 696–707.

Pirity, M.K., Locker, J., and Schreiber-Agus, N. (2005). Rybp/DEDAF is required for early postimplantation and for central nervous system development. Mol. Cell Biol. *25*, 7193–7202.

Roman-Trufero, M., Mendez-Gomez, H.R., Perez, C., Hijikata, A., Fujimura, Y., Endo, T., Koseki, H., Vicario-Abejon, C., and Vidal, M. (2009). Maintenance of undifferentiated state and self-renewal of embryonic neural stem cells by polycomb protein Ring1B. Stem Cells *27*, 1559–1570.

Rose, N.R., King, H.W., Blackledge, N.P., Fursova, N.A., Ember, K.J., Fischer, R., Kessler, B.M., and Klose, R.J. (2016). RYBP stimulates PRC1 to shape chromatin-based communication between Polycomb repressive complexes. eLife *5*, e18591.

Saito, T. (2006). In vivo electroporation in the embryonic mouse central nervous system. Nat. Protoc. *1*, 1552–1558.

Stanton, S.E., Blanck, J.K., Locker, J., and Schreiber-Agus, N. (2007). Rybp interacts with Hippi and enhances Hippi-mediated apoptosis. Apoptosis *12*, 2197–2206.

Stump, G., Durrer, A., Klein, A.L., Lutolf, S., Suter, U., and Taylor, V. (2002). Notch1 and its ligands Delta-like and Jagged are expressed and active in distinct cell populations in the postnatal mouse brain. Mech. Dev. *114*, 153–159.

Szulwach, K.E., Li, X., Smrt, R.D., Li, Y., Luo, Y., Lin, L., Santistevan, N.J., Li, W., Zhao, X., and Jin, P. (2010). Cross talk between microRNA and epigenetic regulation in adult neurogenesis. J. Cell Biol. *189*, 127–141.

Tavares, L., Dimitrova, E., Oxley, D., Webster, J., Poot, R., Demmers, J., Bezstarosti, K., Taylor, S., Ura, H., Koide, H., et al. (2012). RYBP-PRC1 complexes mediate H2A ubiquitylation at polycomb target sites independently of PRC2 and H3K27me3. Cell *148*, 664–678.

Tian, Q., Guo, S.M., Xie, S.M., Yin, Y., and Zhou, L.Q. (2020). Rybp orchestrates spermatogenesis via regulating meiosis and sperm motility in mice. Cell Cycle *19*, 1492–1501.

Tsuboi, M., Hirabayashi, Y., and Gotoh, Y. (2019). Diverse gene regulatory mechanisms mediated by Polycomb group proteins during neural development. Curr. Opin. Neurobiol. *59*, 164–173.

Tsuboi, M., Kishi, Y., Yokozeki, W., Koseki, H., Hirabayashi, Y., and Gotoh, Y. (2018). Ubiquitination-independent repression of PRC1 targets during neuronal fate restriction in the developing mouse neocortex. Dev. Cell *47*, 758–772.e755.

Wu, X., Johansen, J.V., and Helin, K. (2013). Fbxl10/Kdm2b recruits polycomb repressive complex 1 to CpG islands and regulates H2A ubiquitylation. Mol. Cell *49*, 1134–1146.

Xia, W., and Jiao, J. (2017). Histone variant H3.3 orchestrates neural stem cell differentiation in the developing brain. Cell Death Differ. *24*, 1548–1563.

Yao, B., Christian, K.M., He, C., Jin, P., Ming, G.L., and Song, H. (2016). Epigenetic mechanisms in neurogenesis. Nat. Rev. Neurosci. *17*, 537–549.

Zencak, D., Lingbeek, M., Kostic, C., Tekaya, M., Tanger, E., Hornfeld, D., Jaquet, M., Munier, F.L., Schorderet, D.F., van Lohuizen, M., et al. (2005). Bmi1 loss produces an increase in astroglial cells and a decrease in neural stem cell population and proliferation. J. Neurosci. *25*, 5774–5783.

Zhan, S., Wang, T., Ge, W., and Li, J. (2018). Multiple roles of Ring 1 and YY1 binding protein in physiology and disease. J. Cell. Mol. Med. *22*, 2046–2054.

Zhang, R., Engler, A., and Taylor, V. (2018). Notch: an interactive player in neurogenesis and disease. Cell Tissue Res. *371*, 73–89.

Zhao, J., Wang, M., Chang, L., Yu, J., Song, A., Liu, C., Huang, W., Zhang, T., Wu, X., Shen, X., et al. (2020). RYBP/YAF2-PRC1 complexes and histone H1-dependent chromatin compaction mediate propagation of H2AK119ub1 during cell division. Nat. Cell Biol. *22*, 439–452.

Zhou, H., Li, J., Zhang, Z., Ye, R., Shao, N., Cheang, T., and Wang, S. (2016). RING1 and YY1 binding protein suppresses breast cancer growth and metastasis. Int. J. Oncol. *49*, 2442–2452.